Biosensors and Bioelectronics 99 (2018) 1–7

Contents lists available at ScienceDirect

Biosensors and Bioelectronics

journal homepage: www.elsevier.com/locate/bios

An ultrasensitive electrochemical biosensor for polynucleotide kinase assay based on gold nanoparticle-mediated lambda exonuclease cleavage-induced signal amplification

Lin Cui[1], Yueying Li[1], Mengfei Lu[1], Bo Tang, Chun-yang Zhang*

College of Chemistry, Chemical Engineering and Materials Science, Collaborative Innovation Center of Functionalized Probes for Chemical Imaging in Universities of Shandong, Key Laboratory of Molecular and Nano Probes, Ministry of Education, Shandong Provincial Key Laboratory of Clean Production of Fine Chemicals, Shandong Normal University, Jinan 250014, PR China

ARTICLE INFO

Keywords:
Electrochemical biosensor
Signal amplification
Gold nanoparticle-DNA conjugates
Lambda exonuclease cleavage
Polynucleotide kinase activity

ABSTRACT

Polynucleotide kinase (PNK) plays an essential role in cellular nucleic acid metabolism and the cellular response to DNA damage. However, conventional methods for PNK assay suffer from low sensitivity and involve multiple steps. Herein, we develop a simply electrochemical method for sensitive detection of PNK activity on the basis of Au nanoparticle (AuNP)-mediated lambda exonuclease cleavage-induced signal amplification. We use $[Ru(NH_3)_6]^{3+}$ as the electrochemically active indicator and design two DNA strands (i.e., strand 1 and strand 2) to sense PNK. The assembly of strand 2 on the AuNP surface leads to the formation of AuNP-strand 2 conjugates which can be subsequently immobilized on the gold electrode through the hybridization of strand 1 with strand 2 for the generation of a high electrochemical signal. The presence of PNK induces the phosphorylation of the strand 2-strand 1 hybrid and the subsequent cleavage of double-stranded DNA (dsDNA) by lambda exonuclease, resulting in the release of AuNP-strand 2 conjugates and $[Ru(NH_3)_6]^{3+}$ from the gold electrode surface and consequently the decrease of electrochemical signal. The PNK activity can be simply monitored by the measurement of $[Ru(NH_3)_6]^{3+}$ peak current signal. This assay is very sensitive with a detection limit of as low as 7.762×10^{-4} U mL^{-1} and exhibits a large dynamic range from 0.001 to 10 U mL^{-1}. Moreover, this method can be used to screen the PNK inhibitors, and it shows excellent performance in real sample analysis, thus holding great potential for further applications in biological researches and clinic diagnosis.

1. Introduction

DNA phosphorylation plays an important role in many important biological processes, including DNA recombination, DNA replication, and the repair of damaged DNA (Tang et al., 2005; Wang et al., 2002). In the DNA phosphorylation process, polynucleotide kinase (PNK) can catalyze the transfer of the γ-phosphate group of a nucleoside triphosphate to the 5′-hydroxyl termini of nucleic acids (Novogrodsky et al., 1966; Richardson, 1965), and the catalytic activity of PNK is critical to the repairing of DNA strand breaks. Moreover, the human PNK participates in the maintenance of genetic integrity (Rasouli-Nia et al., 2004; Wang et al., 2002) and is closely associated with various human diseases, such as Werner syndrome, Rothmund Thomson syndrome and Bloom's syndrome (Brosh and Bohr, 2007; Sharma et al., 2006). Therefore, accurate detection of PNK activity is of great importance to the biological research and clinical diagnosis.

Conventional methods for PNK assay include radioisotope ^{32}P-labeling (Durand et al., 2012; Lillehaug and Kleppe, 1975a), polyacrylamide gel electrophoresis (Karimi-Busheri et al., 1998) and autoradiography (Phillips and Arlt, 2007). Although these methods are well established, some of them suffer from radioactive contamination and/or labor-intensive procedures. Alternatively, some new approaches such as fluorescent (Huang et al., 2013; Jiao et al., 2012; Lin et al., 2011; Liu et al., 2014a; Song et al., 2015), colorimetric (Jiang et al., 2013, 2014), electrochemical (Cui et al., 2017; Wang et al., 2012, 2013, 2014a) and luminescent assays (Du et al., 2014; He et al., 2014; Tang et al., 2014) have been developed in combination with functional nucleic acid probes (e.g., molecular beacons (He et al., 2014) and DNAzymes (Jiang et al., 2013, 2014; Liu et al., 2014a)) and novel nanomaterials (e.g., graphene oxide (Lin et al., 2011), TiO_2 (Wang et al., 2013, 2014a) and Au nanoparticles (Huang et al., 2013)). The fluorescent method is most widely used for PNK assay, but it usually

* Corresponding author.
E-mail addresses: tangb@sdnu.edu.cn, tangb@sdnu.edu.cn (B. Tang), cyzhang@sdnu.edu.cn, cyzhang@sdnu.edu.cn (C.-y. Zhang).
[1] These authors contributed equally.

http://dx.doi.org/10.1016/j.bios.2017.07.028
Received 8 May 2017; Received in revised form 8 July 2017; Accepted 11 July 2017
Available online 13 July 2017
0956-5663/

relies heavily on the use of functional nucleic acid probes with sophisticated sequence design (Jiao et al., 2012; Liu et al., 2014a; Song et al., 2015) and complicated dye labeling (Shen et al., 2012). The colorimetric method may be carried out with simple and cost-effective instrument, but its sensitivity is usually very poor (Lodeiro et al., 2010). In contrast, the electrochemical method has distinct advantages of low cost, portability and high sensitivity (Wang et al., 2012, 2013, 2014a). Typical electrochemical biosensors for PNK assay are constructed based on either the conjugation of electroactive species (e.g., tyrosine (Kerman et al., 2007) and ferrocene (Wang et al., 2012)) to the substrate (Wang et al., 2012, 2013) or the coordination effect between the phosphate group and the metallic ions (e.g., Ti^{4+} and Zr^{4+}) (Ji et al., 2009; Xu et al., 2009). A detection limit of 0.01 U mL^{-1} can be obtained for an electrochemical biosensor based on Ti^{4+}- and aminoferrocene (Fc)-single wall carbon nanotubes (SWCNTs)-mediated signal amplification, but this biosensor involves complicated preparation of Fc-SWCNTs (Wang et al., 2012). A detection limit of as low as 0.0018 U mL^{-1} has been reported for a label-free electrochemical biosensor based on phosphorylation reaction-triggered exonuclease cleavage, but it may produce a high background electrochemical signal even without target PNK (Zhang et al., 2016b).

Due to their unique optoelectronic properties (e.g., localized surface plasmon resonance (LSPR), huge reactive surface area, unusual catalytic property, fluorescence quenching capability) (Song et al., 2009) and excellent biocompatibility (Guarise et al., 2006), gold nanoparticles (AuNPs) have been widely used for the detection of proteins (Guarise et al., 2006; Wang et al., 2014b; Zhang et al., 2016a,b), nucleic acids (Cao et al., 2002; Seferos et al., 2007; Song et al., 2009), circulating tumor cells (Halo et al., 2014), metal ions (Miao et al., 2013), and intracellular gene (Rosi et al., 2006). Herein, we developed a simple electrochemical biosensor for PNK assay based on AuNP-mediated lambda exonuclease cleavage-induced signal amplification. We used electroactive $Ru(NH_3)_6^{3+}$ as the signal reporter (Zhang et al., 2016a) and designed two DNA strands (i.e., strand 1 and strand 2) to sense PNK. Unlike the reported colorimetric biosensors in which AuNP-DNA conjugates served as the colorimetric reporters (Jiang et al., 2013, 2014), the AuNP-DNA conjugates used in this biosensor may significantly amplify the electrochemical signal, because each AuNP carries a large number of DNA strands which may bind abundant $[Ru(NH_3)_6]^{3+}$ to greatly enhance the electrochemical signals. Moreover, this assay is very rapid and simple without the involvement of time-consuming synthesis procedures and the covalent labeling of oligonucleotides with electroactive (Wang et al., 2012; Wang et al., 2014a) and colorimetric/fluorescent probes (Huang et al., 2013; Jiang et al., 2014; Jiao et al., 2012; Lin et al., 2011; Liu et al., 2014a; Song et al., 2015). This method can be applied for sensitive detection of PNK and screening of PNK inhibitors, and it exhibits excellent performance in real sample analysis as well.

2. Materials and methods

2.1. Materials and reagents

Mercaptohexanol (MCH), tris-(2-carboxyethyl) phosphine hydrochloride (TCEP), tris-(hydroxymethyl)aminomethane (Tris), polysorbate 20 (Tween-20), hexaammineruthenium (III) chloride ($[Ru(NH_3)_6]^{3+}$), bovine serum albumin (BSA), lysozyme, ATP and adenosine diphosphate (ADP) were obtained from Sigma-Aldrich Chemical Co. (St. Louis, MO, USA). T4 polynucleotide kinase (10 U μL^{-1}), lambda exonuclease (5 U μL^{-1}), T4 DNA ligase, E.coli ligase and protein kinase A (PKA) were bought from New England Biolabs (NEB, UK). The AuNPs (10 nm) were purchased from Weiernuode Technology Co. Ltd. (Beijing, China). Other chemicals employed were all of analytical grade and purchased from Sinopharm Chemical Reagent Co. Ltd. (Shanghai, China). The buffers and solutions involved in this research were as follows: DNA immobilization buffer (10 mM PBS, pH 7.4), DNA hybridization buffer (10 mM PBS, 100 mM NaCl, 5 mM $MgCl_2$, pH 7.4), and $[Ru(NH_3)_6]^{3+}$ solution (50 μM $[Ru(NH_3)_6]^{3+}$, 10 mM PBS, 100 mM NaCl, pH 7.4). All solutions were prepared with ultrapure water obtained from a Milli-Q water purification system (Millipore Corp., Bedford, MA, USA) with a resistivity of 18.2 MΩ cm. All of the oligonucleotides (Supplementary information, Table S1) were synthesized and purified with HPLC by Takara Biotech. Co. Ltd. (Dalian, China).

2.2. Apparatus

All electrochemical measurements were carried out on a CHI 660e electrochemical workstation (CH Instruments Inc., USA) at room temperature with a conventional three-electrode system composed of a platinum wire, a saturated calomel and the gold electrode (d = 2 mm) as counter, reference and working electrodes, respectively. Differential pulse voltammetry (DPV) was performed in the potential range from +0.1 to − 0.6 V with 0.05 V amplitude, 0.01 s pulse width and 0.02 s pulse period in the $[Ru(NH_3)_6]^{3+}$ solution. Cyclic voltammetry (CV) measurements were carried out in scanning potential from − 0.2 to 0.6 V with 5 mM $[Fe(CN)_6]^{3-/4-}$ (containing 0.1 M KCl) as the electrolyte. Electrochemical impedance spectroscopic (EIS) measurements were performed in 5 mM $[Fe(CN)_6]^{3-/4-}$ redox couple solution (1:1 M ratio) containing 0.1 M KCl over a frequency range from 10 kHz to 0.1 Hz using an alternative voltage with an amplitude of 10 mV, superimposed on a dc potential of 0.20 V (vs SCE). The chronocoulometry measurements were carried out over a range from +0.2 to − 0.5 V at a pulse period of 250 ms with the $[Ru(NH_3)_6]^{3+}$ as an indicator. The UV–vis absorption spectra were obtained by a Hitachi U-3900 UV–vis spectrophotometer (Varian, USA).

2.3. Preparation of AuNP-DNA conjugates

The AuNP-strand 2 conjugates were synthesized according to the reported protocol (Ding et al., 2010). Briefly, strand 2 was dissolved in 10 mM PBS buffer containing 500 μM TCEP (TCEP was used to reduce the disulfide bonded oligonucleotides) for 30 min. Then strand 2 and the AuNPs (molar ratio of strand 2 to AuNPs is 200:1) were incubated in 10 mM PBS (pH 7.4) containing 0.1% Tween-20 at room temperature with gentle shaking for 16 h to make sure that the AuNPs were fully covered by thiolated strand 2. The colloid solution was salted by stepwise addition of 10 mM PBS containing 3.5 M NaCl and allowed to stand for 40 h. The AuNP-strand 2 conjugates were washed three times with 10 mM PBS (pH 7.4) containing 100 mM NaCl by centrifugation at 13,000 rpm for 30 min to get rid of the unlinked oligonucleotides. The AuNP-strand 2 conjugates were finally redispersed in 10 mM PBS (pH 7.4) containing 100 mM NaCl and stored at 4 °C prior to use.

2.4. Fabrication of electrochemical biosensor

Prior to the modification, the Au electrode was polished to a mirror-like surface with 1.0, 0.3 and 0.05 μm α-Al_2O_3 slurry, respectively, followed by successive sonication with ethanol and ultrapure water for 3 min to remove residual alumina powder. The electrode was then immersed into fresh piranha solution (3:1 v/v mixture of concentrated H_2SO_4 and 30% H_2O_2) for 10 min, followed by a thorough rinse with ultrapure water and drying by nitrogen. Subsequently, the electrode was electrochemically cleaned in 0.1 M H_2SO_4 solution by potential scanning between − 0.2 and +1.6 V at a scan rate of 100 mV s^{-1} until a stable reproducible cyclic voltammogram was obtained. After washing with ultrapure water and drying in a nitrogen stream, the electrode was incubated with 6 μL of 0.5 μM strand 1 which contained 25 μM TCEP (TCEP is used to reduce the disulfide bonded oligonucleotides) at room temperature for 12 h to make strand 1 immobilize onto the gold electrode surface via gold-sulfur chemistry. The electrode was then thoroughly rinsed with 10 mM PBS (pH 7.4) and dried under a stream of nitrogen gas. Subsequently, 6 μL of 1 mM MCH was dropped on the

electrode for 60 min to block the unmodified sites. After rinsing thoroughly with 10 mM PBS (pH 7.4) and dried in nitrogen, the electrode was incubated with AuNP-strand 2 conjugates in 10 mM PBS (pH 7.4) containing 100 mM NaCl at 37 °C for 2 h. At last, the electrode was thoroughly rinsed and dried with nitrogen, and stored at 4 °C prior to use.

2.5. Detection of PNK activity

In a typical phosphorylation assay, the electrochemical biosensor was incubated with 6 μL of PNK reaction buffer containing 1 mM ATP and different-concentration PNK at 37 °C for 30 min. After rinsing with 10 mM PBS (pH 7.4) for three times, 6 μL of lambda exonuclease reaction buffer containing 0.05 U μL^{-1} lambda exonuclease was dropped onto the electrode surface, followed by incubation at 37 °C for 50 min. After washing thoroughly with 10 mM PBS (pH 7.4) for three times, the electrode was placed in 10 mM PBS (pH 7.4) containing 100 mM NaCl and 50 μM $[Ru(NH_3)_6]^{3+}$ for 1 min to reach the equilibrium adsorption of $[Ru(NH_3)_6]^{3+}$. Finally, the electrode was rinsed with the washing buffer for three times prior to the measurement. In addition, the $[Ru(NH_3)_6]^{3+}$ buffer was thoroughly purged with pure nitrogen for 15 min prior to the experiments.

2.6. Inhibition assay

The ADP, NaH_2PO_4 and $(NH_4)_2SO_4$ were used as the model inhibitors in PNK inhibition assay. Similar experimental procedures for PNK assay were employed for PNK inhibition assay except that the inhibitors at various concentrations were pre-mixed with 10 U mL^{-1} PNK reaction buffer.

3. Results and discussion

3.1. Principle of the proposed biosensor

The schematic diagram of the label-free electrochemical biosensor is shown in Scheme 1. We designed two DNA strands (i.e., strand 1 and strand 2), with strand 2 being absorbed on the surface of AuNP to form AuNP-strand 2 conjugates. Strand 1 may function as a capture probe to immobilize the AuNP-strand 2 on the gold electrode through the formation of AuNP-strand 2-strand 1 conjugates. We used $[Ru(NH_3)_6]^{3+}$ as an electrochemically active indicator which can electrostatically absorb on the AuNP-strand 2 and AuNP-strand 2-strand 1 conjugates to generate a high electrochemical signal. In the presence of PNK, the phosphorylation on 5′-terminal of the strand 2-strand 1 hybrid enables the digestion of dsDNA by lambda exonuclease (He et al., 2014; Jiang et al., 2013; Lin et al., 2011), resulting in the release of AuNP-strand 2 conjugates and

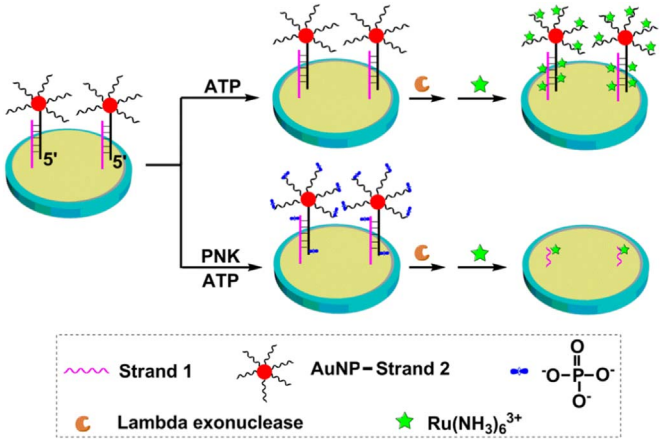

Scheme 1. Schematic illustration of an electrochemical biosensor for PNK assay based on AuNP-mediated lambda exonuclease cleavage-induced signal amplification.

$[Ru(NH_3)_6]^{3+}$ from the gold electrode surface and consequently the decrease of electrochemical signal. The PNK activity can be simply monitored by the measurement of $[Ru(NH_3)_6]^{3+}$ peak current signal. However, in the absence of PNK, neither the phosphorylation nor the lambda exonuclease-mediated digestion of the strand 2-strand 1 hybrid occurs. As a result, neither AuNP-strand 2 conjugates nor $[Ru(NH_3)_6]^{3+}$ can be released from the gold electrode surface, and the electrochemical signal remains unchanged.

3.2. Characterization of AuNP-strand 2 conjugates

We used UV-vis absorption spectroscopy to characterize the AuNP-strand 2 conjugates (Supplementary information, Fig. S1). An absorption peak at 518 nm is observed for 10 nm AuNPs (Supplementary information, Fig. S1A, curve a). After the modification by strand 2, a slight shift in the surface plasmon resonance peak from 518 nm to 522 nm is observed due to the increase of the AuNP diameter induced by the linkage of DNA ligands to the AuNPs (Supplementary information, Fig. S1A, curve b) (Raschke et al., 2003; Xu and Craig, 2007). Notably, a new absorption peak at 260 nm is observed for AuNP-strand 2 conjugates, which is the characteristic absorption peak of the double bond of DNA bases (Zhang et al., 2016a), suggesting the formation of AuNP-strand 2 conjugates. This result is confirmed by the scanning electron microscopy of the AuNP-strand 2 conjugates (Supplementary information, Fig. S2).

3.3. Characterization of electrochemical properties

We employed cyclic voltammograms and electrochemical impedance spectra to characterize the assembly processes of the gold electrode with $[Fe(CN)_6]^{4-/3-}$ as the electroactive probe. In cyclic voltammetric measurements, the peak currents and the separation of peak potential (ΔE_p) changes are used to reflect the electron transfer of redox probe at the sensing interface. As shown in Fig. 1A, the bare gold electrode exhibits a larger redox peak current and a well-defined redox peak of $[Fe(CN)_6]^{3-/4-}$ with a ΔE_p of 96 mV (Fig. 1A, curve a), indicating the fast electron transfer of the redox probe. The self-assembly of strand 1 onto the bare Au electrode causes the decrease of redox peak current and the increase of ΔE_p to 214 mV (Fig. 1A, curve b) due to the blocking of interfacial electron transfer by strand 1. Notably, the surface density of strand 1 on the gold electrode surface is estimated to be 3.94×10^{12} molecules cm^{-2} (Supplementary information, Fig. S3). The subsequent self-assembly of MCH onto the strand 1/Au electrode may block the remaining active sites, resulting in the decrease of redox peak current and the increase of ΔE_p (Fig. 1A, curve c). After further assembly of AuNP-strand 2 onto the MCH/strand 1/Au electrode surface, the negative charged DNA and citrate ligands on the surface of AuNPs may prevent the diffusion of ferricyanide toward the electrode surface, leading to the decrease of redox peak current and the increase of peak-to-peak separation (Fig. 1A, curve d). In the presence of PNK, the PNK-initiated phosphorylation may induce the lambda exonuclease-mediated digestion of dsDNA to release AuNP-strand 2 conjugates from the gold electrode surface, resulting in the increase of peak current and the decrease of ΔE_p (Fig. 1A, curve e).

The electrochemical impedance spectra (EIS) were used for interfacial study (Fig. 1B). The electron-transfer resistance (R_{et}) is controlled by the electron transfer kinetics of $[Fe(CN)_6]^{3-/4-}$ on the modified Au electrodes and may be characterized by the semicircle diameter of Nyquist plot. As shown in Fig. 1B, the bare Au electrode displays a small semicircle diameter and a long tail, indicating the diffusion of $[Fe(CN)_6]^{3-/4-}$ (Fig. 1B, curve a). In contrast, strand 1-modified Au electrode exhibits a higher R_{et} (Fig. 1B, curve b), because the immobilization of negatively charged strand 1 onto the electrode surface may result in a negatively charged interface that electrostatically repels the negatively charged redox probe $[Fe(CN)_6]^{3-/4-}$ and inhibits the interfacial charge transfer. The subsequent surface block-

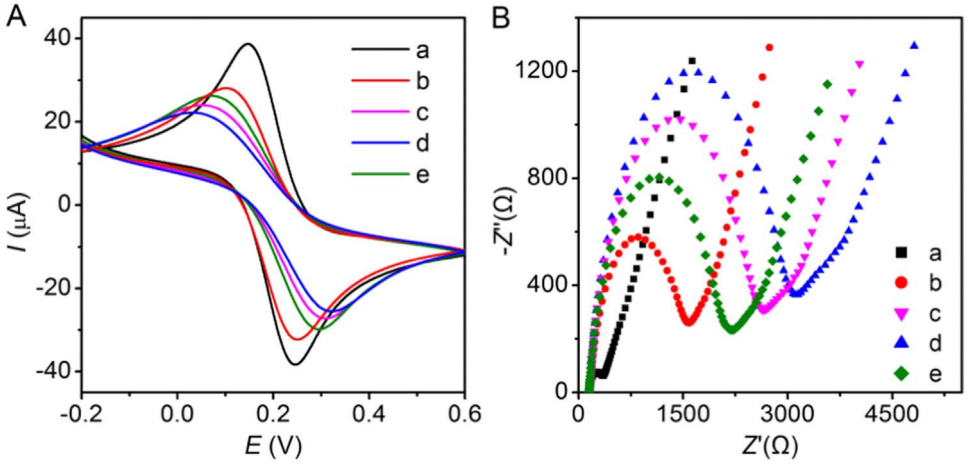

Fig. 1. Cyclic voltammograms (A) and electrochemical impedance spectra (B) of different modified electrodes: (a) bare Au electrode, (b) strand 1/Au electrode, (c) MCH/strand 1/Au electrode, (d) AuNP-strand 2/MCH/strand 1/Au electrode, and (e) the incubation of AuNP-strand 2/MCH/strand 1/Au electrode with 10 U mL^{-1} T4 PNK, 1 mM ATP and 0.05 U μL^{-1} lambda exonuclease.

ing by MCH may induce the increase of R_{et} (Fig. 1B, curve c), because the short alkanethiol provides an insufficient barrier to block electron transfer. After assembly of AuNP-strand 2 onto the MCH/strand 1/Au electrode surface, the electrode interface becomes more negatively charged due to the absorption of negatively charged DNA and citrate ligands onto the AuNP surface, leading to a further increase of R_{et} (Fig. 1B, curve d). On the contrary, the presence of PNK causes significant decrease of R_{et} (Fig. 1B, curve e) due to the release of AuNP-strand 2 conjugates from the gold electrode surface induced by PNK-triggered phosphorylation and lambda exonuclease-mediated digestion of dsDNA. These results clearly demonstrate the success fabrication of electrochemical sensing interface for PNK assay.

3.4. Feasibility of PNK assay

The feasibility of the electrochemical biosensor for PNK assay is confirmed by the measurement of DPV (Fig. 2A). A large DPV peak current signal is observed for the AuNP-strand 2/MCH/strand 1/Au electrode in the absence of PNK (Fig. 2A, curve a) due to the absorption of abundant $[Ru(NH_3)_6]^{3+}$ to the negatively charged phosphate backbone of DNAs. In contrast, a small DPV peak current is observed after incubation with 10 U mL^{-1} PNK, 1 mM ATP and 0.05 U μL^{-1} lambda exonuclease (Fig. 2A, curve b) due to the release of AuNP-strand 2 conjugates and $[Ru(NH_3)_6]^{3+}$ from the gold electrode surface induced by PNK-initiated phosphorylation and lambda exonuclease-mediated digestion. It should be noted that the AuNP-strand 2 conjugates used in this biosensor may significantly amplify the electrochemical signal because each AuNP may assembly a large number of DNA strands for the binding of abundant $[Ru(NH_3)_6]^{3+}$. This is confirmed by a smaller DPV peak current for strand 3/MCH/strand 1/Au electrode without the assembly of AuNP-strand 2 conjugates onto the electrode surface (Fig. 2A, curve c). Interestingly, same DPV peak current is observed for the AuNP-strand 2/MCH/strand 1/Au electrode (Fig. 2A, curve b) and the strand 3/MCH/strand 1/Au electrode (Fig. 2A, curve d) after incubation with 10 U mL^{-1} PNK, 1 mM ATP and 0.05 U μL^{-1} lambda exonuclease, suggesting the complete release of $[Ru(NH_3)_6]^{3+}$ from the gold electrode surface as a result of lambda exonuclease-mediated digestion. Fig. 2B clearly demonstrates that the AuNP-strand 2 conjugates used in this biosensor may significantly amplify the electrochemical signal.

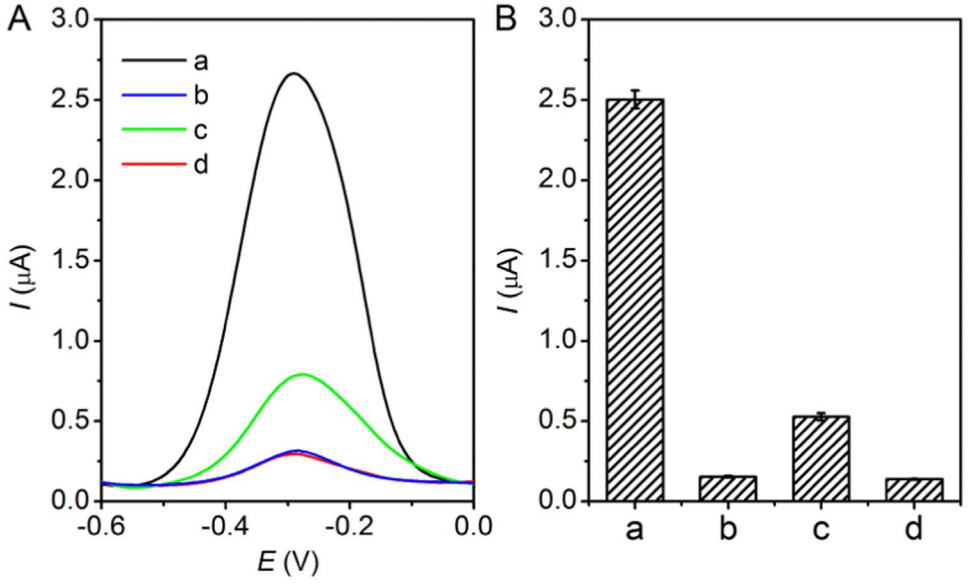

Fig. 2. (A) DPV responses and (B) the comparison of DPV signals for AuNP-strand 2/MCH/strand 1/Au electrode (a, b), strand 3/MCH/strand 1/Au electrode (c, d), before (a, c) and after (b, d) incubation with 10 U mL^{-1} PNK, 1 mM ATP and 0.05 U μL^{-1} lambda exonuclease. The error bars represent the standard deviation of three independent experiments.

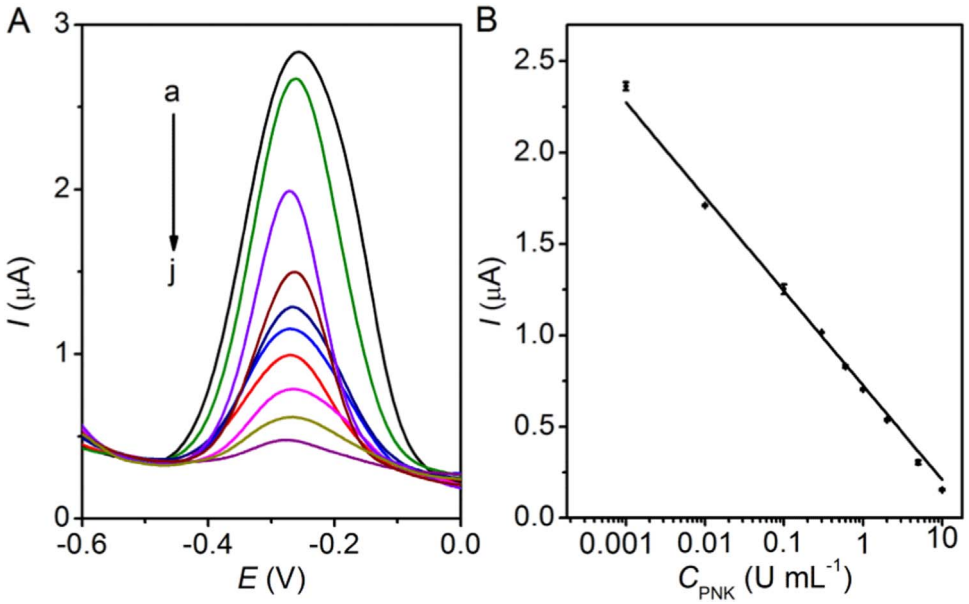

Fig. 3. (A) Measurement of DPV in response to 0, 0.001, 0.01, 0.1, 0.3, 0.6, 1, 2, 5, 10 U mL^{-1} T4 PNK (from a to j) and (B) the linear relationship between the peak current and the concentration of PNK. The ATP concentration is 1.0 mM, and the concentration of lambda exonuclease is 0.05 U μL^{-1}. The error bars represent the standard deviation of three independent experiments.

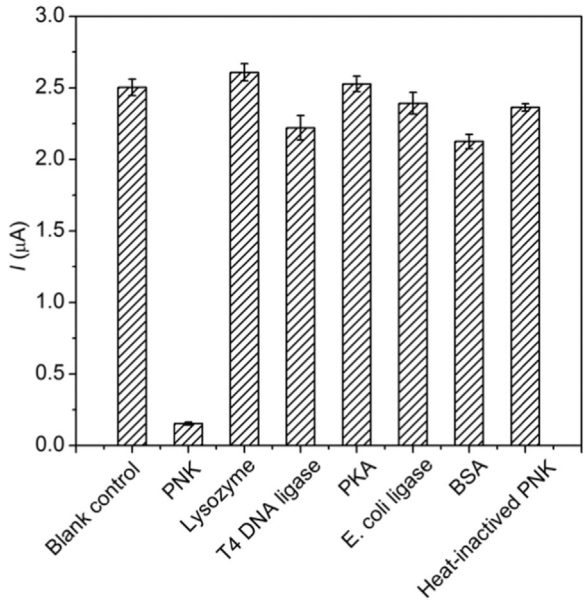

Fig. 4. The specificity of the electrochemical biosensor for PNK assay. [PNK] = 10 U mL^{-1}, [Lysozyme] = 10 μM, [T4 DNA ligase] = 100 U mL^{-1}, [PKA] = 100 U mL^{-1}, [E. coli ligase] = 100 U mL^{-1}, [BSA] = 10 μM, [heat-inactivated T4 PNK] = 10 U mL^{-1}. Error bars represent the standard deviation of three independent experiments.

3.5. Detection of PNK activity

Under the optimally experimental conditions (Supplementary information, Fig. S4), the DPV signal decreases with the increasing concentration of PNK (Fig. 3A). A linear relationship is obtained between the DPV peak current and the logarithm of PNK concentration in the range of 0.001–10 U mL^{-1} (Fig. 3B). The correlation equation is $I = -0.5165 \log_{10} C + 1.778$ ($R^2 = 0.9926$), where I is peak current of the electrochemical biosensor in the presence of PNK, C is the concentration of PNK. The limit of detection (LOD) is calculated to be 7.76×10^{-4} U mL^{-1} by evaluating the average value of the control plus 3 times standard deviation. Notably, the sensitivity of the proposed method is at least 5.3-fold higher than that of bioluminescent assay (Du et al., 2014), 2.4-fold higher than those of reported electrochemical methods (Hou et al., 2014; Lin et al., 2012; Miao et al., 2011; Peng et al., 2013; Wang et al., 2012, 2013, 2014a; Zhang et al., 2016b), 2.4-fold higher than those of colorimetric methods (Jiang et al., 2013, 2014), 1.3-fold higher than that of photoelectrochemical method (Zhuang et al., 2015) and 1.3-fold higher than those of fluorescent method (Hou et al., 2013; Jiao et al., 2012; Lin et al., 2011; Liu et al., 2014b; Ma et al., 2013; Song et al., 2015; Tao et al., 2015; Zhou et al., 2015) (Supplementary information, Table S2). The high sensitivity of the proposed method may be ascribed to both the signal amplification effect of AuNP-DNA conjugates and the efficient cleavage of phosphorylated dsDNA by lambda exonuclease. Moreover, we demonstrated that this method can be used for sensitive detection of PNK activity in cell extracts (Supplementary information, Fig. S5).

3.6. Detection specificity

To investigate the specificity of the proposed method, we measured T4 PNK, the heat-inactivated T4 PNK and some irrelevant proteins including PKA, lysozyme, T4 DNA ligase, E. coli ligase and BSA. Among them, BSA, lysozyme, T4 DNA ligase and E. coli ligase cannot catalyze the transfer of γ-phosphate group of a nucleoside triphosphate to the 5′-hydroxyl termini of nucleic acids (Jiang et al., 2014; Tao et al., 2015). The PKA can catalyze the transfer of phosphate from gamma position of ATP to serine hydroxyl group of the substrate peptides, generating the phosphorylated peptides (Wang et al., 2015). A shown in Fig. 4, the DPV peak current remains unchanged in the presence of irrelevant proteins and the heat-inactivated T4 PNK. In contrast, the presence of T4 PNK induces significant decrease in the DPV peak current, suggesting the high specificity of the proposed method for T4 PNK assay.

3.7. PNK inhibition assay

We used ADP, Na_2HPO_4 and $(NH_4)_2SO_4$ as the model inhibitors to investigate the feasibility of the proposed method for PNK inhibition assay. These inhibitors show no inhibition effect on the activity of lambda exonuclease (Hou et al., 2013). The inhibition efficiency (E) is calculated on the basis of $E = (1 - I_i/I_0) \times 100\%$, where I_i is the DPV peak current in the presence of inhibitors, and I_0 is the DPV peak

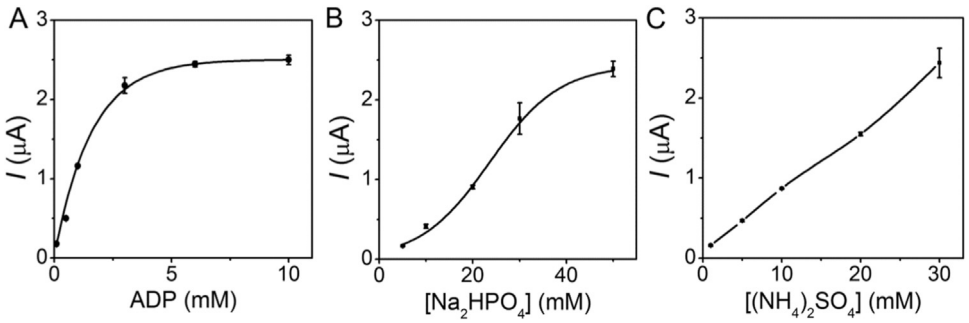

Fig. 5. Inhibitory effects of (A) ADP, (B) Na_2HPO_4 and (C) $(NH_4)_2SO_4$ upon PNK activity. The error bars represent the standard deviation of three independent experiments.

current in the absence of inhibitors. The coexistence of ADP with 5′-phosphorylated nucleic acids may trigger a reversible phosphorylation reaction, making the phosphate of DNA transfer to ADP molecule and inducing inhibition effect on PNK activity (Hou et al., 2013; Tang et al., 2005). As shown in Fig. 5A, the DPV peak current improves with the increasing concentration of ADP, and the half-maximal inhibition concentration (IC_{50}) (Hou et al., 2014) of ADP is calculated to be 1.12 mM, consistent with those obtained by chemiluminescent (1.32 mM) (Tang et al., 2014) and electrochemical (1 mM) (Lin et al., 2012) methods. Previous research demonstrated that Na_2HPO_4 and $(NH_4)_2SO_4$ may inhibit the activity of PNK through the salt effect on the phosphorylation reaction (Lillehaug and Kleppe, 1975b; Lillehaug et al., 1976). As shown in Fig. 5B-C, the DPV peak current improves with the increasing concentrations of Na_2HPO_4 and $(NH_4)_2SO_4$, respectively. The IC_{50} value is calculated to be 23 mM for Na_2HPO_4 and 15 mM for $(NH_4)_2SO_4$, consistent with the reported IC_{50} value of 24 mM for Na_2HPO_4 and 9.88 mM for $(NH_4)_2SO_4$ obtained by the bioluminescent assay (Du et al., 2014), 20 mM for Na_2HPO_4 and 10 mM for $(NH_4)_2SO_4$ obtained by the fluorescent assay (Lin et al., 2011). These results clearly demonstrate the feasibility of the proposed method for the screening of PNK inhibitors.

4. Conclusions

In summary, we have developed a new electrochemical biosensor for sensitive and selective detection of PNK based on AuNP-mediated lambda exonuclease cleavage-induced signal amplification. We used $[Ru(NH_3)_6]^{3+}$ as the electrochemically active indicator and designed two DNA strands to sense PNK. The presence of PNK induces the phosphorylation of DNA and the subsequent cleavage of dsDNA by lambda exonuclease, resulting in the release of AuNP-DNA conjugates and $[Ru(NH_3)_6]^{3+}$ from the gold electrode surface and consequently the decrease of electrochemical signal. Unlike the reported colorimetric biosensors in which AuNP-DNA conjugates served as the colorimetric reporters (Jiang et al., 2013, 2014), the AuNP-DNA conjugates used in this biosensor may significantly amplify the electrochemical signal due to the adsorption of abundant $[Ru(NH_3)_6]^{3+}$ onto each AuNP-DNA conjugate. Moreover, this assay is very rapid and simple without the involvement of time-consuming synthesis procedures and the covalent labeling of oligonucleotides with electroactive and colorimetric/fluorescent probes. This method is very sensitive with a low detection limit of as low as 7.76×10^{-4} U mL^{-1}, which is superior to the reported electrochemical, photoelectrochemical, bioluminescent, colorimetric and fluorescent methods (described in the section of detection of PNK activity) for PNK assay. Importantly, this electrochemical biosensor can be applied for the screening of PNK inhibitors and accurate quantification of PNK in cell extracts, showing great promise in clinic diagnosis and drug discovery.

Acknowledgments

This work was supported by the National Natural Science Foundation of China (Grant Nos. 21325523, 21527811 and 21605096), and the Award for Team Leader Program of Taishan Scholars of Shandong Province, China.

Appendix A. Supplementary material

Supplementary data associated with this article can be found in the online version at doi:10.1016/j.bios.2017.07.028.

References

Brosh, R.M., Bohr, V.A., 2007. Nucleic Acids Res. 35, 7527–7544.
Cao, Y.C., Jin, R., Mirkin, C.A., 2002. Science 297, 1536–1540.
Cui, L., Lu, M.F., Yang, X.Y., Tang, B., Zhang, C.Y., 2017. Analyst 142, 1562–1568.
Ding, B., Deng, Z., Yan, H., Cabrini, S., Zuckermann, R.N., Bokor, J., 2010. J. Am. Chem. Soc. 132, 3248–3249.
Du, J., Xu, Q.F., Lu, X.Q., Zhang, C.-Y., 2014. Anal. Chem. 86, 8481–8488.
Durand, S., Richard, G., Bontems, F., Uzan, M., 2012. Proceedings Natl. Acad. Sci. USA. 109, 7073–7078.
Guarise, C., Pasquato, L., De Filippis, V., Scrimin, P., 2006. Proceedings Natl. Acad. Sci. USA. 103, 3978–3982.
Halo, T.L., McMahon, K.M., Angeloni, N.L., Xu, Y., Wang, W., Chinen, A.B., Malin, D., Strekalova, E., Cryns, V.L., Cheng, C., 2014. Proceedings Natl. Acad. Sci. USA. 111, 17104–17109.
He, H.-Z., Leung, K.-H., Wang, W., Chan, D.S.-H., Leung, C.-H., Ma, D.-L., 2014. Chem. Commun. 50, 5313–5315.
Hou, T., Wang, X.Z., Liu, X.J., Lu, T.T., Liu, S.F., Li, F., 2013. Anal. Chem. 86, 884–890.
Hou, T., Wang, X., Liu, X., Pan, C., Li, F., 2014. Sens. Actuators B: Chem. 202, 588–593.
Huang, Y., Chen, J., Shi, M., Zhao, S., Chen, Z.-F., Liang, H., 2013. J. Mater. Chem. B 1, 2018–2021.
Jiang, C., Yan, C., Jiang, J., Yu, R., 2013. Anal. Chim. Acta 766, 88–93.
Jiang, H.-X., Kong, D.-M., Shen, H.-X., 2014. Biosens. Bioelectron. 55, 133–138.
Jiao, H.P., Wang, B., Chen, J., Liao, D.L., Li, W.Y., Yu, C., 2012. Chem. Commun. 48, 7862–7864.
Ji, J., Yang, H., Liu, Y., Chen, H., Kong, J., Liu, B., 2009. Chem. Commun., 1508–1510.
Karimi-Busheri, F., Lee, J., Weinfeld, M., Tomkinson, A.E., 1998. Nucleic Acids Res. 26, 4395–4400.
Kerman, K., Vestergaard, M. d., Tamiya, E., 2007. Anal. Chem. 79, 6881–6885.
Lillehaug, J.R., Kleppe, K., 1975a. Biochemistry 14, 1221–1225.
Lillehaug, J.R., Kleppe, K., 1975b. Biochemistry 14, 1225–1229.
Lillehaug, J.R., Kleppe, R.K., Kleppe, K., 1976. Biochemistry 15, 1858–1865.
Lin, L., Liu, Y., Yan, J., Wang, X., Li, J., 2012. Anal. Chem. 85, 334–340.
Lin, L., Liu, Y., Zhao, X., Li, J.H., 2011. Anal. Chem. 83, 8396–8402.
Liu, S.F., Ming, J.J., Lin, Y., Wang, C.F., Cheng, C.B., Liu, T., Wang, L., 2014a. Biosens. Bioelectron. 55, 225–230.
Liu, S.F., Ming, J.J., Lin, Y., Wang, C.F., Liu, T., Cheng, C.B., Li, F., 2014b. Sens. Actuators B: Chem. 192, 157–163.
Lodeiro, C., Capelo, J.L., Mejuto, J.C., Oliveira, E., Santos, H.M., Pedras, B., Nuñez, C., 2010. Chem. Soc. Rev. 39, 2948–2976.
Ma, C.B., Fang, H.F., Wang, K.M., Xia, K., Chen, H.C., He, H.L., Zeng, W.M., 2013. Anal. Biochem. 443, 166–168.
Miao, P., Ning, L.M., Li, X.X., 2013. Anal. Chem. 85, 7966–7970.
Miao, P., Ning, L.M., Li, X.X., Shu, Y.Q., Li, G.X., 2011. Biosens. Bioelectron. 27, 178–182.
Novogrodsky, A., Tal, M., Traub, A., Hurwitz, J., 1966. J. Biol. Chem. 241, 2933–2943.
Peng, Y.L., Jiang, J.H., Yu, R.Q., 2013. RSC Adv. 3, 18128–18133.
Phillips, D.H., Arlt, V.M., 2007. Nat. Protoc. 2, 2772–2781.
Raschke, G., Kowarik, S., Franzl, T., Sönnichsen, C., Klar, T., Feldmann, J., Nichtl, A., Kürzinger, K., 2003. Nano Lett. 3, 935–938.
Rasouli-Nia, A., Karimi-Busheri, F., Weinfeld, M., 2004. Proceedings Natl. Acad. Sci. USA. 101, 6905–6910.
Richardson, C.C., 1965. Proceedings Natl. Acad. Sci. USA. 54, 158–165.
Rosi, N.L., Giljohann, D.A., Thaxton, C.S., Lytton-Jean, A.K., Han, M.S., Mirkin, C.A., 2006. Science 312, 1027–1030.

Seferos, D.S., Giljohann, D.A., Hill, H.D., Prigodich, A.E., Mirkin, C.A., 2007. J. Am. Chem. Soc. 129, 15477–15479.
Sharma, S., Doherty, K.M., Brosh, R.M., 2006. Biochem. J. 398, 319–337.
Shen, W., Deng, H., Gao, Z., 2012. J. Am. Chem. Soc. 134, 14678–14681.
Song, C.X., Yang, X.H., Wang, K.M., Wang, Q., Liu, J.B., Huang, J., He, L.L., Liu, P., Qing, Z.H., Liu, W., 2015. Chem. Commun. 51, 1815–1818.
Song, S.P., Liang, Z.Q., Zhang, J., Wang, L.H., Li, G.X., Fan, C.H., 2009. Angew. Chem. Int. Ed. 48, 8670–8674.
Tang, Z., Wang, K., Tan, W., Ma, C., Li, J., Liu, L., Guo, Q., Meng, X., 2005. Nucleic Acids Res. 33, (e97–e97).
Tang, W., Zhu, G.C., Zhang, C.-Y., 2014. Chem. Commun. 50, 4733–4735.
Tao, M.J., Shi, Z.L., Cheng, R., Zhang, J., Li, B.X., Jin, Y., 2015. Anal. Biochem. 485, 18–24.
Wang, L.K., Lima, C.D., Shuman, S., 2002. EMBO J. 21, 3873–3880.
Wang, L.J., Yang, Y., Zhang, C.Y., 2015. Anal. Chem. 87, 4696–4703.
Wang, G., Chen, L., He, X., Zhu, Y., Zhang, X., 2014a. Analyst 139, 3895–3900.
Wang, G., He, X., Xu, G., Chen, L., Zhu, Y., Zhang, X., Wang, L., 2013. Biosens. Bioelectron. 43, 125–130.
Wang, Y., He, X., Wang, K., Ni, X., Su, J., Chen, Z., 2012. Biosens. Bioelectron. 32, 213–218.
Wang, Z., Sun, N., He, Y., Liu, Y., Li, J., 2014b. Anal. Chem. 86, 6153–6159.
Xu, J., Craig, S.L., 2007. Langmuir 23, 2015–2020.
Xu, X.H., Nie, Z., Chen, J.H., Fu, Y.C., Li, W., Shen, Q.P., Yao, S.Z., 2009. Chem. Commun., 6946–6948.
Zhang, H., Dong, H.L., Yang, G.Q., Chen, H.F., Cai, C.X., 2016a. Anal. Chem. 88, 11108–11114.
Zhang, Q.M., Li, Z., Zhou, Y.L., Li, X., Li, B.C., Yin, H.S., Ai, S.Y., 2016b. Sens. Actuators B: Chem. 225, 151–157.
Zhou, L., Shen, X.Q., Sun, N., Wang, K.M., Zhang, Y.Y., Pei, R.J., 2015. Analyst 140, 5450–5453.
Zhuang, J.Y., Lai, W.Q., Xu, M.D., Zhou, Q., Tang, D.P., 2015. ACS Appl. Mater. Interfaces 7, 8330–8338.